Methods in Ecology and Evolution

British Ecological Society

Methods in Ecology and Evolution doi: 10.1111/j.2041-210X.2012.00208.x

Distorted-distance models for directional dispersal: a general framework with application to a wind-dispersed tree

Bram van Putten[1]*, Marco D. Visser[2,3], Helene C. Muller-Landau[2] and Patrick A. Jansen[2,4]

[1]*Mathematical and Statistical Methods Group, Wageningen University, PO Box 100, 6700 AC Wageningen, The Netherlands;* [2]*Smithsonian Tropical Research Institute, Apartado 0843-03092, Balboa, Ancón, Panama;* [3]*Department of Experimental Plant Ecology, Radboud University Nijmegen, PO Box 9010, 6500 GL Nijmegen, The Netherlands; and* [4]*Department of Environmental Sciences, Wageningen University, PO Box 47, 6700 AA Wageningen, the Netherlands*

Summary

1. Seed and pollen dispersal is often directionally biased, because of the inherent directionality of wind and many other dispersal vectors. Nevertheless, the vast majority of studies of seed and pollen dispersal fit isotropic dispersal kernels to data, implicitly assuming that dispersal is equally likely in all directions.

2. Here, we offer a flexible method for stochastic modelling of directional dispersal data. We show how anisotropic models can be constructed by combining standard dispersal functions with 'distorted-distance functions' that transform the circular contour lines of any isotropic dispersal kernel into non-circular shapes. Many existing anisotropic phenomenological models of seed and pollen dispersal are special cases of our framework.

3. We present functional forms for the specific case of elliptic distorted-distance functions, under which contour lines of the seed shadow become non-concentric, nested ellipses, and show how models using these functions can be constructed and parameterized. R-code is provided.

4. We applied the elliptic anisotropic models to characterize seed dispersal in the wind-dispersed Neotropical tree *Luehea seemannii* (Malvaceae) on Barro Colorado Island, Panama. We used inverse modelling to fit alternative models to data of seed rain into seed traps, the locations of seed traps and adult trees, and tree size.

5. Our anisotropic model performed considerably better than commonly applied isotropic models, revealing that seed dispersal of *L. seemannii* was strongly directional. The best-fitting model combined a 3-parameter elliptic distorted-distance function that captured the strong directional biases with a 1-parameter exponential dispersal kernel, a 1-parameter negative binomial probability distribution describing the clumping of seed rain and a 1-parameter function relating tree fecundity to tree diameter.

6. The framework presented in this paper enables more flexible and accurate modelling of directional dispersal data. It is applicable not only to studies of seed dispersal, but also to a wide range of other problems in which large numbers of particles disperse from one or more point sources.

Key-words: anisotropic model, dispersal kernel, inverse modelling, *Luehea seemannii*, Matrushka property, pollen dispersal, ray-convex set, seed dispersal, seed shadow, stochastic model

Introduction

Dispersal is one of the central themes of modern plant biology, and patterns of seed and pollen dispersal are important to the ecology, biogeography and genetic structure of plant populations and communities (Nathan & Muller-Landau 2000; Trakhtenbrot *et al.* 2005). Despite its fundamental importance, seed and pollen dispersal remains poorly understood, mainly because they are difficult to quantify. Dispersing seeds and pollen grains are notoriously hard to follow, and dispersed seeds (or pollen) can be unambiguously linked to source plants only in exceptional situations (Wang & Smith 2002), e.g. when

*Correspondence author. E-mail: bram.vanputten@wur.nl

there is only one source within dispersal range or when genetic markers identify a sole possible source (Robledo-Arnuncio & Garcia 2007, Jones & Muller-Landau 2008). A second major challenge is the appropriate mathematical description of observed dispersal patterns in terms of dispersal kernels – the probability distributions of distances and directions of dispersal (Cousens, Dytham & Law 2008).

Mathematical description has been particularly challenging because dispersal of seeds, of other plant propagules and of pollen is often directional. For example dispersion patterns generated by wind are strongly biased by prevailing wind directions (Tackenberg 2003; Wagner *et al*. 2004), whereas dispersion patterns generated by animal seed dispersers and pollinators often have directional components as a result of the configuration of the landscape and the non-randomness of animal behaviour (Levine & Murrell 2003; Contreras Sánchez, Greene & Quesada 2011). This directionality is important to plant populations and communities. Directional bias fundamentally reduces the degree to which dispersal spreads seeds (or pollen) around in space, as seeds from the same source end up closer together than they would under non-directional dispersal (Wright *et al*. 2008), and thus reduces the benefits of dispersal, specifically the benefits related to reduced kin competition and bet hedging over environmental heterogeneity (Levin *et al*. 2003). Despite the ubiquity and importance of directional dispersal, most mathematical descriptions of dispersal have focused exclusively on dispersal distances, ignoring direction by applying isotropic models. This can lead to serious overestimation of dispersal distances in some directions and underestimation in others, and calls for models incorporating directionality (Contreras Sánchez, Greene & Quesada 2011).

Though most studies of dispersal use isotropic kernels, anisotropic kernels have been used to describe seed and pollen dispersal in a dozen publications (including Prat 1995; Burczyk, Adams & Shimizu 1996; Tufto, Engen & Hindar 1997; Bullock & Clarke 2000; Staelens *et al*. 2003; Tackenberg 2003; Wagner *et al*. 2004; Soons *et al*. 2005; Kuparinen 2006; Austerlitz *et al*. 2007; Skarpaas & Shea 2007; Soubeyrand *et al*. 2007; Soons & Bullock 2008; Soubeyrand, Enjalbert & Sache 2008; Soubeyrand *et al*. 2009; Wälder, Näther & Wagner 2009; Savage *et al*. 2011; Skarpaas *et al*. 2011). Some of these publications, as well as others, have introduced mechanistic and quasi-mechanistic models with directional effects (Okubo & Levin 1989; Nathan, Safriel & Noy-Meir 2001; Stockmarr 2002; Klein *et al*. 2003; Katul *et al*. 2005; Nathan *et al*. 2011). However, the anisotropic phenomenological models developed to date have limited flexibility. Existing models describe directionality in specific kernels and do not allow for directionality to be incorporated with other dispersal distance distributions.

Here, we present a general framework that makes it possible to develop anisotropic versions of any dispersal kernel. Under this framework, an anisotropic kernel is a combination of two functions: a dispersal distance distribution that may relate to a traditional isotropic dispersal kernel, and a 'distorted-distance' function that accounts for directional biases. Our framework enables the construction of an endless variety of anisotropic dispersal kernels, because any dispersal distance distribution can be combined with any kind of distorted-distance functions. We first present the general framework. We then provide functional forms for one class of distorted-distance functions, the elliptic distorted-distance model. Next, we apply elliptic distorted-distance models to fit seed dispersal distances in a wind-dispersal Neotropical tree on Barro Colorado Island (BCI), Panama, through inverse modelling. Finally, we discuss the results, compare our approach with previous work on anisotropic dispersal, give recommendations and outline potential applications in fields other than seed dispersal. In the Appendices, we provide relevant proofs, methodological details and R-code for fitting and simulating our models.

A general framework for modelling directional dispersal

Seed shadows under any isotropic model with arbitrary dispersal kernel function d can be characterized by concentric *circular* contour lines of seed density around the seed source (Clark *et al*. 1999). Our framework for anisotropic dispersal is to 'distort' these contours into one (or more) directions into which dispersal is biased, e.g. as a result of the prevailing wind direction(s) at the time(s) seeds are released. Such distortions can be quite complex and reflect multiple effects (Fig. 1). The result, characterized by non-concentric contour lines, is an *an*isotropic model, accounting for directional effects in seed dispersal.

Consider the simplest case of seed dispersal away from a single point source, tree 'A', located in $(\hat{x}, \hat{y})$ of a rectangular X–Y plane. Our anisotropic model for the final location of a seed dispersed randomly from this point has probability density function (pdf) p, the 2D dispersal kernel', and consists of two sub-models. The first is a deterministic model r_{dist} that describes the so-called distorted distance $r_{\text{dist}}(x, y)$ to tree A for each location (x, y) in the plane around the tree, the 'distorted-distance mapping'. The second is a stochastic model that describes the probability distribution of distorted distances for a seed dispersed from tree A, in the form of a (one-dimensional) pdf d, the 'distorted-distance distribution'. The

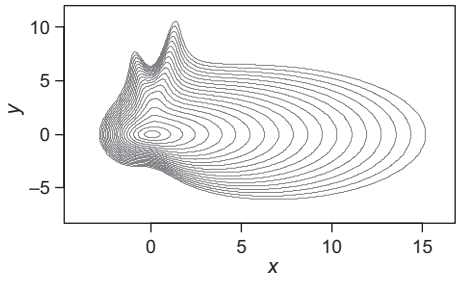

Fig. 1. A hypothetical seed shadow resulting from seed dispersal by wind blowing from multiple directions, described with the modelling framework presented in the main text; the contour lines show seed densities. The corresponding distorted-distance function is given in Appendix B.

parameters of functions d and r_{dist} can be estimated from field data.

The two-dimensional dispersal kernel p is a function of location (x, y) only through its distorted distance $r_{\text{dist}}(x, y)$ to tree A, so that locations with equal distorted distances to the tree have equal probability density: $p(x_1, y_1) = p(x_2, y_2)$ if $r_{\text{dist}}(x_1, y_1) = r_{\text{dist}}(x_2, y_2)$. As a consequence, contour lines of r_{dist} and p coincide, although their respective values on a contour will of course differ. The distorted-distance mapping r_{dist} specifically and fully describes the directional component, whereas the distorted-distance distribution d specifies the probability that a seed lands at distorted distance r_{dist} from the seed source, yet itself contains no information about how distances are distorted.

A variety of isotropic dispersal kernel functions have been successfully fit to field data (e.g. Clark *et al.* 2005). In *iso*tropic modelling, where dispersal is assumed equally likely is all directions, the contour lines of the two-dimensional dispersal kernel p take the form of concentric circles centred at the tree source. We can think of this two-dimensional dispersal kernel as reflecting the combination of an (undistorted) Euclidean distance mapping

$$r_{\text{Eucl}}(x, y) = \sqrt{(x - \hat{x})^2 + (y - \hat{y})^2}$$

with an (undistorted) distance distribution d. Our *an*isotropic model can incorporate the same mathematical functions d in the form of distorted-distance distributions, and combine these with a distorted-distance mapping r_{dist} in place of the Euclidean distance function. The resulting distorted distances $r_{\text{dist}}(x, y)$ can have contour lines that are distorted rings (e.g. an ellipse) or even indented/outdented ovals (e.g. Fig. 1).

Under our framework, there are two general ways in which dispersal kernels can be directionally distorted. First, the distorted distance in one direction can be different from the distorted distance in another direction – that is, the contour lines take some form other than circles centred at the source location. In the simplest case, these contours are ellipses sharing the same centre and are characterized by a direction and a degree of eccentricity. Secondly, the centre of the distribution of dispersed seeds (the point at which the effective distance is zero) can be shifted away from the source. This shift is captured by a shift vector, $\Delta = (\Delta_x, \Delta_y)$, consisting of a shift Δ_x in the X-direction and a shift Δ_y in the Y-direction. The resulting (unique) imaginary source centre $\left(\hat{x}^*, \hat{y}^*\right) = (\hat{x} + \Delta_x, \hat{y} + \Delta_y)$ has the property that $r_{\text{dist}}\left(\hat{x}^*, \hat{y}^*\right) = 0$. The shift vector can equivalently be characterized in polar coordinates, by its magnitude δ and its angle θ with the positive X-axis. Note that both types of distortion lead to differences in the proportions of seeds going in different directions from the source, in addition to changing the distribution of distances travelled by seeds going in different directions.

Although an endless variety of possible r_{dist} functions can be specified, we will impose several (in many applications natural) restrictions. First, the contour lines of r_{dist} must have a single unique imaginary source centre. Secondly, the contour lines of r_{dist} should have a so-called ray-convex interior so that the straight line connecting the imaginary source centre $(\hat{x}^*, \hat{y}^*)$ with an arbitrary point on a contour line never crosses that contour line in any point (Olieman & van Putten 2010). Thirdly, contour lines should expand continuously with $r = r_{\text{dist}}$, starting from the imaginary source centre, implying that they fully enclose each other. We say that a distorted-distance mapping that meets the three abovementioned conditions has the 'Matrushka property.' A mathematical formulation of this property is given in Appendix A.

Even distorted-distance mappings that produce indented and outdented contour lines can satisfy the Matrushka property (e.g. Fig. 1). Such distorted-distance functions could arise if for example seed dispersal is depressed in a certain direction because the influence of an obstacle. Examples of ray-convex (but not convex) seed shadows are given in Wagner *et al.* (2004; fig. 10); Soubeyrand *et al.* (2007; figs. 4–7) and in this paper (Figs 1 and 2a). Although the Matrushka property implies that points *within* a contour line have lower distorted distances than points *on* that contour line, it remains possible that the two-dimensional dispersal kernel, and thus the seed shadow, is higher on contour lines of higher distorted distance (e.g., Staelens *et al.* 2003 fig. 3; Wagner *et al.* 2004 fig. 6; Cousens, Dytham & Law 2008 figs 5.1, 5.3, and 5.18).

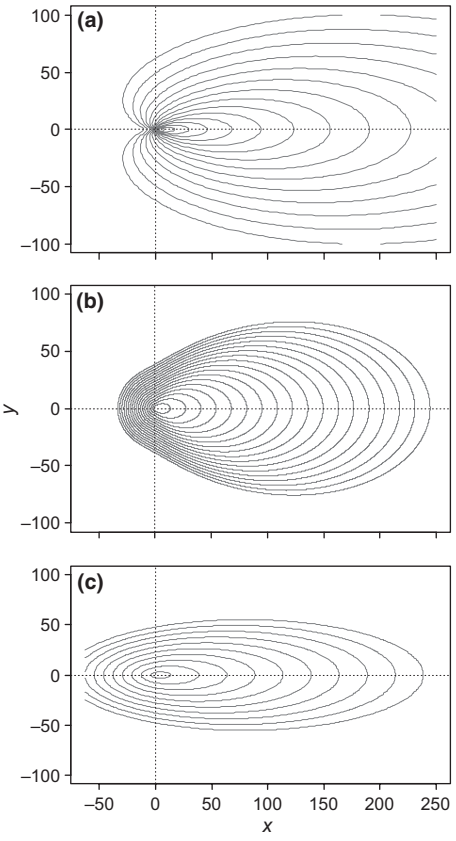

Fig. 2. Contour lines of three seed shadows, generated with distorted-distance models, that correspond with three existing anisotropic phenomenological models: (a) Tufto, Engen & Hindar (1997), formula 19 with $\lambda_0 = 0.05$, $\theta_0 = 0$ and $\kappa = 10$; (b) Wagner *et al.* (2004), formulas 11 and 12 with $k = 1$, $u = -\pi$ and $v = -1$; (c) Staelens *et al.* (2003), formula 5 with $c_0 = 1$, $c_1 = 0.5$ and $\theta_d = -\pi/2$.

We call a distorted-distance mapping 'non-concentric' if the interiors of the ovals representing the contour lines do not have the same barycentre (centre of mass). These functions may 'drift' in a certain direction, i.e. the direction into which the barycentres move as ovals expand. Figures 2a–c all show a drift in the direction of the positive X-axis. The full elliptic distortion model described in the next section is another example of a distorted distance exhibiting a drift. A distorted distance is called 'concentric' if all contour line ovals have a common barycentre, i.e. no drift.

Directional seed dispersal kernels generated by this framework can be compared in terms of their mean ovals and their quantile ovals, which are the 2D planar counterparts of the 1D mean and the 1D quantile dispersal distances. The mean oval O_{Ed} is defined as the oval for which each point is the mean of seed dispersal distance in the ray starting from the imaginary source centre in the direction of that point. Similarly, the median oval O_{med} is defined as the oval for which each point is the (1D) median of the seed dispersal in the ray starting from the imaginary source centre into the direction of that point. Note that it thus contains 50% of the modelled seed deposition. Although the latter property is shared with many other ovals in the plane, the median oval is unique in the sense that it is an oval *contour line* having this property. Quantile ovals can be defined similarly, i.e. the p-quantile oval is the (unique) contour line having the property that its interior contains $p \times 100\%$ of the modelled seed deposition, leaving $(1 - p) \times 100\%$ outside the oval ($0 \leq p < 1$). If the kernel is monotone, decreasing with the distorted distance, then the area within the p-quantile oval is the (unique) smallest area in the plane having the latter property. Formal definitions of 2D mean and 2D quantile ovals and methods for calculating them, as well as formulas for the calculation of the 1D mean and 1D median of the Euclidean distance to the (original) seed source, are given in Appendix A.

The elliptic distorted-distance model

Here, we present a relatively simple yet flexible distorted-distance model that produces elliptic contour lines (concentric or non-concentric). The full version of this model has five scalar parameters: Δ_x, Δ_y, ψ, β and γ (Table 1). The 'shift' vector $\Delta = (\Delta_x, \Delta_y)$ describes the displacement of the imaginary source centre from the source. The rotation parameter ψ ($-\pi < \psi \leq \pi$) describes the angle of the common axis of the expanding elliptic contour lines with the positive X-axis (Fig. 3). The coherency parameter β ($\beta > 0$) determines the eccentricity of the elliptic contour lines: the higher β, the more the contours lines are flattened along that common axis (compare Fig. 4a–c). Finally, the drift parameter γ ($\gamma \geq 0$) pulls the ellipses into the positive direction along the common axis (Fig. 3): the higher γ, the higher the directional effect (compare Fig. 4a,d,g). Reduced versions of the model utilize subsets of these parameters (Table 1). The most reduced version models isotropic dispersal.

For convenience, we first define the coordinates of the imaginary source centre as $\left(\hat{x}^*, \hat{y}^*\right) = (\hat{x} + \Delta_x, \hat{y} + \Delta_y)$. Then, the distorted-distance mapping for the full elliptic distortion model is

$$r^{\mathrm{ELL}}_{\mathrm{dist};\beta,\gamma,\psi,\Delta_x,\Delta_y}(x,y) = f^{\mathrm{ELL}}_{\beta,\gamma}\Big((x-\hat{x}^*)\cos\psi + (y-\hat{y}^*)\sin\psi,\ (x-\hat{x}^*)\sin\psi - (y-\hat{y}^*)\cos\psi\Big),$$

where

$$f^{\mathrm{ELL}}_{\beta,\gamma}(x,y) = \sqrt{(2\gamma^2+1)\left(\frac{x^2}{\beta^2}+\frac{2\gamma x}{\beta}\right)+(\gamma^2+1)(y^2+2\gamma^2)-2\gamma\left(\frac{x}{\beta}+\gamma\right)\sqrt{(\gamma^2+1)\left[\left(\frac{x}{\beta}+\gamma\right)^2+y^2+1\right]}}$$

(proof in Appendix B). Contour lines in the full elliptic distortion model are non-concentric ellipses and the elliptic distortion distance fulfils the Matrushka property (proof in Appendix C). The ellipses are a generalization of ellipses applied in a geophysical context (Wheeler 1984).

The value of the two-dimensional dispersal kernel $p(x, y)$ for each location (x, y) in the plane is a function of its distorted distance $r = r_{\mathrm{dist}}(x, y)$ and the value $d(r)$ of the distorted-distance distribution. In the full elliptic distortion model, the two-dimensional dispersal kernel p^{ELL} is expressed in terms of the distorted-distance distribution d as

$$\begin{aligned} p^{\mathrm{ELL}}(x,y) &= p^{\mathrm{ELL}}_{\beta,\gamma,\psi,\Delta_x,\Delta_y}(x,y) \\ &= \frac{\Omega^{\mathrm{ELL}}}{r^{\mathrm{ELL}}_{\mathrm{dist}}(x,y)}\, d\left(r^{\mathrm{ELL}}_{\mathrm{dist}}(x,y)\right), \end{aligned} \qquad \text{eqn 1}$$

where

$$\Omega^{\mathrm{ELL}} = \frac{1}{2\pi\beta\sqrt{\gamma^2+1}}$$

(proof in Appendix D). The special case in which ellipses are circles has $\beta = 1$, $\gamma = 0$ and ψ undefined. Equation 1 then reduces to $p(x, y) = (1/2\pi r_{\mathrm{dist}}(x, y))\, d(r_{\mathrm{dist}}(x, y))$ in which

$$r_{\mathrm{dist}}(x,y) = r_{\mathrm{Eucl}}(x-\hat{x}^*, y-\hat{y}^*) = \sqrt{(x-\hat{x}^*)^2+(y-\hat{y}^*)^2}$$

is the Euclidean distance to the imaginary source centre.

The elliptic distortion model can be generalized into a multimodal model in two different ways. First, a multimode generalization can be constructed as a mixture of a finite number of full elliptic distortion models pointing in different directions,

Table 1. Parameters in the elliptic distorted-distance model, their names, effects and possible reduction

Parameter	Range	Name	Effect	Reduction
ψ (psi)	$-\pi < \psi \leq \pi$ (radians)*	Rotation angle	Rotates the seed shadow around the imaginary source centre $\left(\tilde{x}^*, \tilde{y}^*\right)$ over angle ψ	Undetermined when $\beta = 1$ and $\gamma = 0$ (isotropy around the imaginary source centre)
β (beta)	$\beta > 0$	Coherency	Flattens the contour lines along their common axis	$\beta = 1$ (requires $\gamma = 0$) means contour lines are circular
γ (gamma)	$\gamma \geq 0$	Drift	Pulls the centres of contour lines into the positive direction of the common axis (set by ψ)	$\gamma = 0$ means all contour lines have the same centre
$\Delta = (\Delta_x, \Delta_y)$† (delta)	$-\infty < \Delta_x < \infty$, $-\infty < \Delta_y < \infty$	Shift	Translates the seed shadow to the imaginary source centre $\left(\tilde{x}^*, \tilde{y}^*\right)$ where the distorted distance equals zero	$\Delta_y = \Delta_x \tan(\psi)$ sets the shift angle equal to the rotation angle $\Delta = (0, 0)$ means that the imaginary source centre is at the source

*Note that $\psi = 0$ points to East, and $\psi = -\pi/2$ points to South.
†Alternatively, in polar coordinates, $\Delta = (\delta, \theta)$, with length $\delta \geq 0$ and angle $-\pi < \theta \leq \pi$. The accompanying reduction is $\theta = \psi$, forcing the shift angle to be the same as the rotation angle.

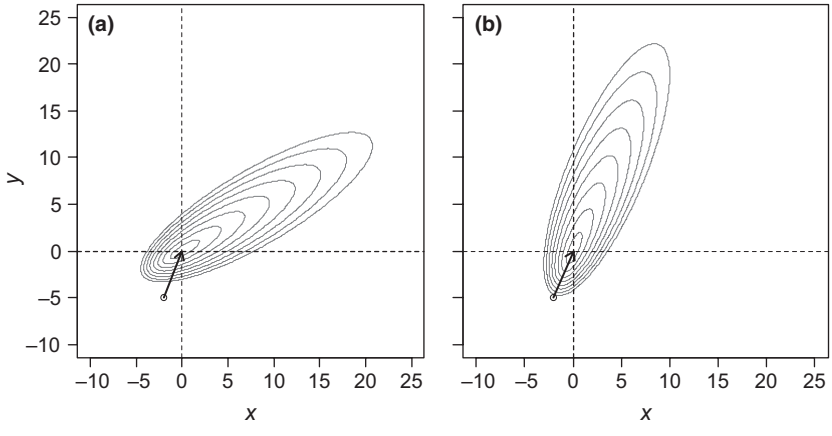

Fig. 3. Contour lines of the hypothetical seed shadow of a single tree produced by the full elliptic distortion model, including rotation and shift in different directions (a) or in the same direction (b). In both cases, the shift vector is $\Delta = (2, 5)$, the tree is located in $(-2, -5)$ and the imaginary source centre is located at $(\tilde{x}^*, \tilde{y}^*) = (0, 0)$. The model shown has coherence $\beta = 2$, drift $\gamma = 1.5$ and rotation $\psi = \pi/6$ (a) or rotation $\psi = \arctan(5/2)$ (b).

with a common imaginary source centre (identical Δ_x and Δ_y). This construction is similar to the one proposed in Savage *et al.* (2011). Alternatively, a multimodal model can be generated by substituting appropriate functions of x and y respectively into the elliptic distorted-distance function, leading to (non-elliptic) extensions of the elliptic model, including multimode distorted distances. Appendix B concludes with one such example (the one shown in Fig. 1).

Model choice and parameter estimation

Dispersal kernels can be estimated from empirical data on the distributions of dispersed seeds (Eulerian methods) or on the trajectories of dispersing seeds (Lagrangian methods) (Bullock, Shea & Skarpaas 2006). The Eulerian approach is more common and typically involves counting the numbers of seeds in seed traps in different positions relative to one or more seed sources. Estimation of seed dispersal kernels from such data requires also specifying a probability distribution for observed seed number as a function of expected seed number (an error distribution), which in the simplest case is the Poisson distribution (e.g., Ribbens, Silander & Pacala 1994). In addition, when the numbers of seeds dispersing from each seed source are not known, one must also fit a model for seed production. Thus in practice, the complete model will often include four sub-models: (1) distorted-distance mapping, (2) distorted-distance distribution, (3) seed production and (4) error distribution.

In practice, parameter estimation is often based on seed distribution data from scenarios with multiple seed sources, such as seed rain captured by seed traps that are scattered through a forest with many reproductive trees. For an arbitrary location (x, y) in the field, the distorted distance $r_{\text{dist},i}$ to source i is a function of the distance to that source and parameters β_i, γ_i, ψ_i, $\Delta_{x,i}$, $\Delta_{y,i}$ for that source as outlined above. The two-dimensional dispersal kernel p_i of source i depends on these distorted-distance parameters and on the form and parameters of the distorted-distance distribution d_i, which can vary among trees (Fig. 5). Clearly, model complexity can be greatly reduced if one or more parameters are assumed equal for all sources. Parameter reduction can also be achieved by relating parameters to other measured attributes of sources. For example fecundity may be proportional to plant size, and the shift may be proportional to plant height. For the elliptic model in particular, the number of parameters can be further reduced in many practical situations by assuming that the

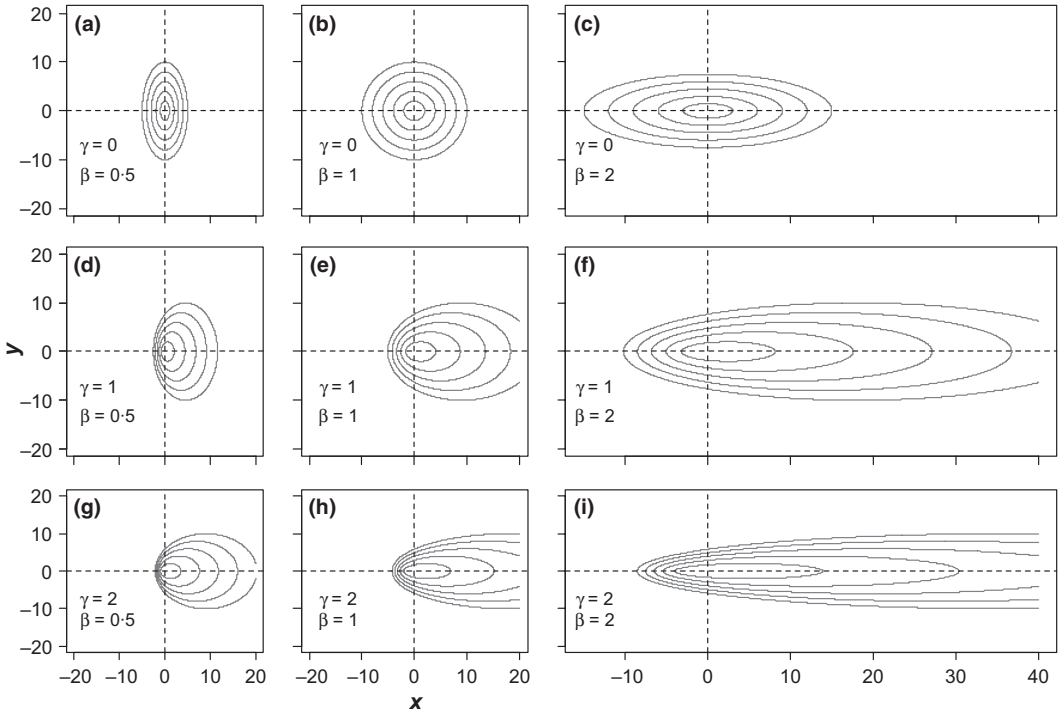

Fig. 4. Contour lines of hypothetical seed shadows around a single imaginary source centre, generated with the elliptic distortion model using different parameter values. The coherency parameter increases from left to right, flattening the distribution contours. The drift parameter increases from top to bottom, and increases the degree to which the ellipse centres move into the rotation direction. In all cases, the imaginary source centre is at (0, 0) and the rotation parameter is 0.

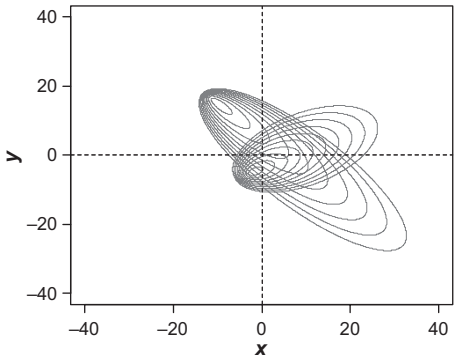

Fig. 5. Contour lines of the hypothetical seed shadows of two trees when parameters of the elliptic distortion model differ between the trees. Parameter values for the first tree are $(\bar{x}_1^*, \bar{y}_1^*) = (-10\ ,\ 15)$, $\psi_1 = -\pi/4$, $\gamma_1 = 3$, $\beta_1 = 1$; for the second tree, they are $(\bar{x}_2^*, \bar{y}_2^*) = (-2\ ,\ -5)$, $\psi_2 = \pi/6$, $\gamma_2 = 1{\cdot}5$, $\beta_2 = 1$. This situation could arise if the two trees released seeds at different times, under different wind conditions.

rotation and shift are in the same direction (Fig. 2). This is a sensible restriction in many cases, as when prevailing winds shift and stretch the seed distributions of all trees into a single direction.

We briefly mention here the risk of over-parameterisation. For example when $\gamma = 0$ and $\beta = 1$, distorted-distance contour lines reduce to circles around the imaginary source centre, and thus the rotation parameter ψ is undetermined (all values result in the same distorted-distance mapping). Similarly, when $\gamma = 0$, the exact same contour lines can be obtained by changing eccentricity β to $1/\beta$ and simultaneously increasing or decreasing the rotation by $\pi/2$ (Fig. 4a,c). In cases like these, additional parameter reductions or constraints are needed.

Application to a wind-dispersed tree

We fitted our anisotropic elliptic models to data for the wind-dispersed canopy tree *Luehea seemannii* (Malvaceae) in tropical moist forest on BCI, Panama (Leigh 1999). We used diameters and locations of all *L. seemannii* ≥ 200 mm DBH (Diameter at Breast Height) in the 2005 censuses of a 50-ha Forest Dynamics Plot (FDP) in the centre of the island (Condit 1998) plus a 10-ha buffer area directly to the north of the FDP, totalling 60 ha (600 × 1000 m). Seed distribution data were numbers of mature *L. seemannii* seeds captured by 200 litter traps, each 0·5 m^2 in area, in the FDP during 2004–2010 (7 years) (Fig. 6; for details, see Muller-Landau *et al.* 2008).

We fitted alternative seed shadows using inverse modelling, calculating expected seed rain into each trap by summing expected seed rain from all source trees on the plot (Appendix E; Ribbens, Silander & Pacala 1994; Jones & Muller-Landau 2008). We assumed that all trees had the same two-dimensional dispersal kernel, and fitted 12 alternative models for this kernel, representing all combinations of four distorted (or undistorted)-distance mappings and three distorted (or undistorted)-distance distributions. The four elliptic distorted-

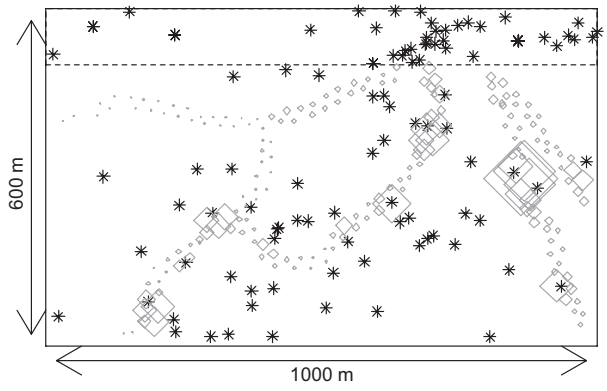

Fig. 6. Map of the study area on Barro Colorado Island, Panama, showing the locations of reproductive *Luehea seemannii* trees (asterisks) and of the seed traps (squares). Symbols of seed traps are scaled by the number of *L. seemannii* seeds they captured [specifically, to $\log_{10}$(seed number + 1)].

Table 2. Functional forms of the distorted-distance distributions (probability density functions for the distribution of distorted distances) fitted to the seed dispersal data in the case study

Distribution	Functional form
Exponential	$d(r) = \frac{1}{\lambda} e^{-r/\lambda}$
1-parameter Weibull*	$d(r) = \frac{2r}{\lambda^2} e^{-r^2/\lambda^2}$
1-parameter Student's 2DT†	$d(r) = \frac{4r}{\lambda(1 + (r^2/\lambda))^2}$

Note that when combined with Euclidean distance mappings, these are (undistorted) distance distributions, i.e. one-dimensional dispersal kernels. All functions have a single parameter $\lambda > 0$, with increasing values of this parameter associated with increasing dispersal distances, and are defined only for $r \geq 0$.
*With shape parameter set equal to 2.
†With degrees of freedom parameter set to 2; this is equivalent to the kernel defined in Clark *et al.* (1999) equation 8 when $p = 2$.

distance models were (1) the *full* 5-parameter elliptic model (parameters ψ, β, γ, Δ_x, Δ_y); (2) the 4-parameter *constrained shift* model in which the rotation is in the direction of the shift [free parameters ψ, β, γ, Δ_x with $\Delta_y = \Delta_x \tan(\psi)$]; (3) the 3-parameter *no shift* model (free parameters ψ, β, γ with $\Delta_x = 0$, $\Delta_y = 0$) and (4) the 0-parameter *isotropic* model (with $\Delta_x = 0$, $\Delta_y = 0$, $\beta = 1$, $\gamma = 0$ and no role for ψ). The three different distorted-distance distributions were the (1-parameter) Exponential, the 1-parameter Weibull and the 1-parameter Student's 2DT (Table 2). We assumed the fecundity of tree i, φ_i was related to its diameter, z_i, as $\varphi_i = \alpha z_i^2$, and we thus fit a single fecundity parameter, α. We assumed that observed values followed a negative binomial distribution around the expected, with clumping parameter κ taking lower values when clumping is greater (Clark, Macklin & Wood 1998).

For each model, we numerically searched for the parameter values that maximized the likelihood of the observed seed trap data using the Nelder–Mead downhill simplex method (Nelder & Mead 1965; R Development Core Team 2011). We compared model performance using Akaike's (1974) Information Criterion (AIC). Finally, we simulated 100 seed trap datasets for this population using the best-fit model and parameters, ran our fitting procedure for these simulated datasets and quantified the bias and precision of the resulting parameter estimates. The full R-code for the fits and the simulation are given in Appendices R and S respectively.

Results

The anisotropic models all provided better fits than the corresponding isotropic models (Table 3). The best-fitting model combined an exponential dispersal kernel function with the 'no shift' elliptic distorted-distance function. The contour lines of expected seed rain (Fig. 7a) show pronounced directionality. The mean and median dispersal distances predicted by the

Table 3. Alternative models of seed dispersal in the wind-dispersed tree *Luehea seemannii* (Malvaceae) on Barro Colorado Island, Panama, fitted to data of seed rain into seed traps and the spatial distribution of seed traps and adult trees using inverse modelling

ΔAIC	No. of pars	Distorted-distance model	Distribution	Distance λ	Rotation ψ	Coherency β	Drift γ	Shift in X Δ_x	Shift in Y Δ_y	Fecundity* α	Clumping κ
0	6	No shift	Exponential	23·3	−0·453	1·049	0·938	*0*	*0*	2·22	0·991
1·403	8	Full	Exponential	23·3	−0·416	1·120	0·876	0·370	1·997	2·20	1·004
1·712	7	Constrained shift	Exponential	23·1	−0·454	1·041	0·951	0·354	*−0·173*	2·23	0·996
27·24	6	No shift	2DT	2202	−0·387	0·752	1·038	*0*	*0*	1·95	0·881
27·58	7	Constrained shift	2DT	2196	−0·390	0·706	1·177	1·754	*−0·721*	1·95	0·891
28·23	8	Full	2DT	2201	−0·262	0·825	0·925	−4·212	5·134	1·92	0·883
67·07	6	No shift	Weibull	29·5	−0·645	2·576	0·420	*0*	*0*	2·01	0·719
68·17	7	Constrained shift	Weibull	28·9	−0·643	2·709	0·402	−0·894	*0·670*	1·97	0·758
69·28	8	Full	Weibull	28·5	−0·641	2·770	0·399	1·150	1·926	1·95	0·763
103·8	3	Isotropic	Exponential	32·7		*1*	*0*	*0*	*0*	2·30	0·642
114·3	3	Isotropic	2DT	2670		*1*	*0*	*0*	*0*	2·18	0·616
143·7	3	Isotropic	Weibull	55·8		*1*	*0*	*0*	*0*	2·13	0·549

The models are combinations of four elliptic distortion functions, with different levels of reduction, and three distorted distance distributions. Models are ranked by ΔAIC, the difference in Akaike Information Criterion from the best-fit model. Parameter values that are italicized were constrained to that value.
*The estimated fecundity of a tree is this parameter times the square of its diameter in millimetre.

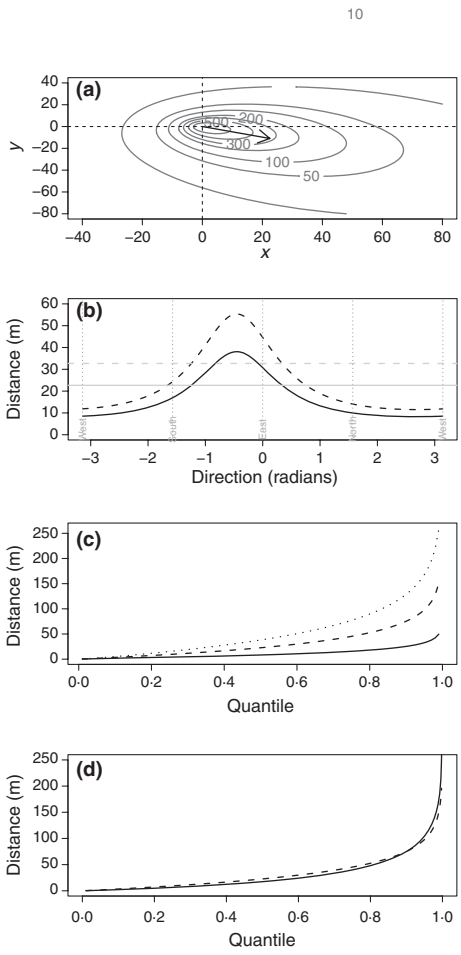

Fig. 7. Characteristics of the best-fit seed dispersal model for the tropical forest tree *Luehea seemannii* (Malvaceae) on Barro Colorado Island, estimated from tree location and seed trap data through inverse modelling. (a) Contour lines of the expected seed rain (absolute seed density per m^2) according to the best-fit (and anisotropic) model for a hypothetical tree of DBH = 500 mm. The vector shows the prevailing direction, ESE. (b) Mean (dashed lines) and median (solid lines) dispersal distance from the source centre for different directions for the anisotropic model (black lines) compared to the best-fitting isotropic model (grey lines). (c) The maximum (dotted line) and minimum (solid line) distances travelled at a given quantile for the anisotropic model, when maxima and minima are taken over directions, compared with the distance for the same quantile under the isotropic model (dashed line). (d) The Euclidean distance at a given quantile when all directions are combined under the anisotropic model (solid line) vs. the isotropic model (dashed line).

best-fitting isotropic kernel were 32·7 and 22·7 m respectively. The estimated mean dispersal distance in the best-fitting anisotropic model ranged from 11·5 to 55·4 m depending on the direction, with an overall mean of 24·1 m (Fig. 7b), whereas the median ranged from 8·3 to 38·1 depending on direction, with an overall value of 16·8 m. Thus, the distorted mean and median dispersal distance varied greatly with direction (Fig 7a,b). All anisotropic models found that seeds going east-southeast travelled the longest distances (Fig. 7a,b).

The directional variation in dispersal distances under the best-fit anisotropic model is evident in the contrast between the directional maximum and directional minimum dispersal distance as a function of quantile, with this range encompassing wide variation around the quantile distances of the isotropic model (Fig. 7c). The probability distribution of Euclidean distances travelled in all directions combined under the best-fit anisotropic model was nonetheless quite similar to that for the isotropic model, as evident from the similarity in distances as a function of quantile (Fig. 7d). The main difference between the distributions was in the tail, which in the anisotropic case is fatter because of the relatively higher probability of long-distance seed dispersal into the preferred direction. Methods for quantifying directional variability in the elliptic distortion model are provided in Appendix F.

Fits to the simulated datasets recovered the true parameter values very well (Table 4). Mean bias did not exceed 12% of the true parameter value and root mean squared errors did not exceed 36% of the true parameter value for the distance, coherency, drift, fecundity and clumping parameters. In the case of the rotation parameter ψ, proportionality calculations are nonsensical, and the mean bias was 0·02 radians. In all cases, the 95% confidence intervals of the fitted parameters included the true values.

Discussion

We have outlined a flexible framework for stochastic modelling of directional dispersal data, in which standard dispersal functions are combined with 'distorted-distance functions' that transform the circular contour lines of any isotropic dispersal kernel into non-circular shapes reflecting directional biases. Application to a field problem – estimating seed dispersal in the wind-dispersed Neotropical forest tree *L. seemannii* – demonstrated that anisotropic models can be fit to a typical dataset. Our model effectively detected anisotropy in this species' seed shadow, fitted an appropriate distance distortion and estimated directionality that was consistent with wind dispersal. Our estimate of the median dispersal distance of *L. seemannii* averaged over directions (16·8 m) closely matched the estimate of Muller-Landau *et al.* (2008; median = 17 m), despite methodological differences, and are just slightly higher than those in Dalling *et al.* (2002; median = 8.2 m).

We introduced 2D analogues for the commonly used 1D versions of mean, median and *p*-quantiles of the dispersal distribution. The 1D and 2D versions are useful to address different questions. The 1D versions address the question of how far seeds (or pollen and the like) are dispersed from the source. The 2D versions provide insight into the underlying process and, in particular, into the variability in dispersal distributions in different directions from the imaginary source centre.

COMPARISON TO OTHER APPROACHES

Three general approaches for mathematically capturing directionality in phenomenological models of dispersal have previously been published. The simplest approach assumes that the dispersal kernel is bivariate normal (Austerlitz *et al.* 2007). Because such distributions necessarily have concentric ellipti-

Table 4. Fit statistics for 100 simulated datasets with the same form as the empirical dataset (R-code in Appendices S and R)

Statistic	Distance λ	Rotation ψ	Coherency β	Drift γ	Fecundity α	Clumping κ
Generating parameter value	23·30	−0·45	1·05	0·94	2·22	0·99
Mean estimated value	25·62	−0·43	1·02	1·05	2·13	1·01
Median estimated value	24·52	−0·44	1·00	0·99	2·12	0·98
95% CI estimated value	19·97, 48·21	−0·57, −0·27	0·53, 1·68	0·60, 1·88	1·83, 2·43	0·76, 1·45
Root mean squared error	6·00	0·07	0·28	0·34	0·18	0·16
Mean bias	2·32	0·02	−0·03	0·11	−0·09	0·02
Mean proportional bias	0·10	NA	−0·03	0·12	−0·04	0·02
95% CI proportional bias	−0·14, 1·07	NA	−0·50, 0·60	−0·36, 1·00	−0·18, 0·09	−0·24, 0·46

The generating model, the exponential, had a lower Akaike Information Criterion score than any competing kernel model in all simulations.

cal contour lines for given probabilities of seed arrival (e.g., Hogg, McKean & Craig 2012), these models are special cases of our elliptic distortion model, without shift or drift. A second approach has been to use a direction-dependent intensity function (Wälder, Näther & Wagner 2009). This approach produces shifted concentric ellipses and again is a special case of our elliptic model, with shift but without drift. The third and final general approach uses the Von Mises distribution or a related distribution, a common tool in circular statistics (Batschelet 1981). Here, the kernel function contains a radially dependent component, usually a translated sine function, to account for directional effects. Tufto, Engen & Hindar (1997), Staelens *et al*. (2003) and Wagner *et al*. (2004) for example all apply a (generalized) Von Mises distribution, but differ in the way the distribution enters the formulas. All these phenomenological models are special cases of our general framework (see Appendix G for ad hoc proofs regarding the models in Tufto, Engen & Hindar (1997), Staelens *et al*. (2003) and Wagner *et al*. (2004); see also Fig. 2).

Our approach of combining a distorted-distance mapping with a 1D probability density function for distorted distance has parallels with the framework proposed by Schurr, Steinitz & Nathan (2008) for handling 'path effects'. Path effects of environments encountered by dispersing seeds (or pollen) can slow or speed dispersal at different distances in different directions around a given source, and thus effectively distort distances in a manner similar to our approach. Schurr, Steinitz & Nathan (2008) describe path effects using the notion of a 'movement space'; distances in this movement space parallel our notion of 'distorted distance', and the mapping to movement space parallel our distorted-distance mapping. Schurr, Steinitz & Nathan (2008) specifically consider the simplified case in which path effects 'depend only on the environments crossed by the straight line extending from the source to the deposition site', a restriction that means that all of their 'movement distance' functions satisfy our 'Matrushka property' for distorted-distance mappings. Thus, the model formulated by Schurr, Steinitz & Nathan (2008) can be considered a special case of our framework. Our framework is more general in that it does not specify a particular mechanism as responsible for distorting distances, and thus encompasses not only path effects but also effects such as those of the distribution of wind speed and direction, effects that may be uniform across the landscape.

Our modelling framework has several advantages. First, directional effects can be fully accounted for in r_{dist}, so that function d deals exclusively with the non-directional effects, and all parameters are distinctly directional or non-directional. Secondly, modelling is very flexible as many functions d and r_{dist} are possible and can be independently combined. Contour lines, including their shape, can be 'estimated' from field data, and an appropriate distorted distance could be defined or adapted accordingly. Previous phenomenological models have less flexibility and cannot accommodate as wide a range of possible distributions. In practice, this means that our model framework will often produce superior fits to data. This is illustrated by our application, in which our model fitted the seed distribution data substantially better than did the models given by Austerlitz *et al*. (2007) and Wälder, Näther & Wagner (2009), because of our inclusion of drift parameter γ.

Conclusion

We have described a method for converting any isotropic dispersal kernel into an anisotropic dispersal kernel, and demonstrated how such kernels can be fit to empirical data. Anisotropic kernels constructed in this framework fitted data on a wind-dispersed tree species far better than did isotropic models. Application of this model should increase accuracy and precision in estimates of dispersal distances, enable estimation of the direction of movement and thus allow better description and prediction of the dispersal and distribution of seeds and other particles.

Our method is suited for a wide variety of situations in which particles disperse away from point sources, particularly where this dispersal is passive, involving wind or water. The quantity of interest can be discrete, such as the number of particles, as well as continuous, e.g. a concentration. Examples include the dispersal of coral gametes in oceans, roots in soil, volcanic ash in air and wind dispersed pollution deposition from single or multiple point sources. The notions of tree, fecundity, etc., can be easily translated into the relevant terminology. Expression of models in these various areas using a common statistical framework would facilitate exchange of models between appli-

cations, and recombination of functional forms to best fit observed distributions.

Acknowledgements

We thank the Associate Editor and two anonymous referees for valuable comments that improved the manuscript. This study was supported by the Netherlands Foundation for Scientific Research (NWO-ALW 863-07-008 to PAJ; NWO-ALW 801-01-009 to MDV), the Smithsonian Tropical Research Institute (MDV), the HSBC Climate Partnership (HML) and the C.T. de Wit Graduate School for Production Ecology and Resource Conservation (HML). The case study datasets were collected with funding from the National Science Foundation (DEB 0614255, 0453665, 0640386, 0425651, 0346488, 0129874, 00753102, 9909347, 9615226, 9615226, 9405933, 9221033, 9100058, 8906869, 8605042, 8206992, 792219), the Smithsonian Tropical Research Institute, the Centre for Tropical Forest Science, the John D. and Catherine T. MacArthur Foundation, the Mellon Foundation and the Small World Institute Fund.

References

Akaike, H. (1974) A new look at the statistical model identification. *IEEE Transactions on Automatic Control*, **19**, 716–723.

Austerlitz, F., Dutech, C., Smouse, P., Davis, F. & Sork, V. (2007) Estimating anisotropic pollen dispersal: a case study in *Quercus lobata*. *Heredity*, **99**, 193–204.

Batschelet, E. (1981) *Circular Statistics in Biology*. Academic Press, London.

Bullock, J.M. & Clarke, R.T. (2000) Long distance seed dispersal by wind: measuring and modelling the tail of the curve. *Oecologia*, **124**, 506–521.

Bullock, J.M., Shea, K. & Skarpaas, O. (2006) Measuring plant dispersal: an introduction to field methods and experimental design. *Plant Ecology*, **186**, 217–234.

Burczyk, J., Adams, W.T. & Shimizu, J.Y. (1996) Mating patterns and pollen dispersal in a natural knobcone pine (*Pinus attenuate* Lemmon.) stand. *Heredity*, **77**, 251–260.

Clark, J.S., Macklin, E. & Wood, L. (1998) Stages and spatial scales of recruitment limitation in Southern Appalachian forests. *Ecological Monographs*, **68**, 213–235.

Clark, J.S., Silman, M., Kern, R., Macklin, E. & HilleRisLambers, J. (1999) Seed dispersal near and far: patterns across temperate and tropical forests. *Ecology*, **80**, 1475–1494.

Clark, C.J., Poulsen, J.R., Bolker, B.M., Connor, E.F. & Parker, V.T. (2005) Comparative seed shadows of bird-, monkey-, and wind-dispersed trees. *Ecology*, **86**, 2684–2694.

Condit, R. (1998) *Tropical Forest Census Plots: Methods and Results from Barro Colorado Island, Panama and a Comparison with Other Plots*. Springer, Berlin.

Contreras Sánchez, J.M., Greene, D.F. & Quesada, M. (2011) A field test of inverse modeling of seed dispersal. *American Journal of Botany*, **98**, 698–703.

Cousens, R., Dytham, C. & Law, R. (2008) *Dispersal in Plants: a Population Perspective*. Oxford University Press, Oxford.

Dalling, J.W., Muller Landau, H.C., Wright, S.J. & Hubbell, S.P. (2002) Role of dispersal in the recruitment limitation of neotropical pioneer species. *Journal of Ecology*, **90**, 714–727.

Hogg, R.V., McKean, J.W. & Craig, A.T. (2012) *Introduction to Mathematical Statistics*, 7th edn. Pearson, Boston, Mass.

Jones, F.A. & Muller-Landau, H.C. (2008) Measuring long-distance seed dispersal in complex natural environments: an evaluation and integration of classical and genetic methods. *Journal of Ecology*, **96**, 642–652.

Katul, G., Porporato, A., Nathan, R., Siqueira, M., Soons, M., Poggi, D., Horn, H. & Levin, S. (2005) Mechanistic analytical models for long-distance seed dispersal by wind. *American Naturalist*, **166**, 368–381.

Klein, E.K., Lavigne, C., Foueillassar, X., Gouyon, P.-H. & Larédo, C. (2003) Corn pollen dispersal: quasi-mechanistic models and field experiments. *Ecological Monographs*, **73**, 131–150.

Kuparinen, A. (2006) Mechanistic models for wind dispersal. *Trends in Plant Science*, **11**, 296–301.

Leigh, E.G. (1999) *Tropical Forest Ecology: a View from Barro Colorado Island*. Oxford University Press, New York.

Levin, S.A., Muller-Landau, H.C., Nathan, R. & Chave, J. (2003) The ecology and evolution of seed dispersal: a theoretical perspective. *Annual Review of Ecology, Evolution, and Systematics*, **34**, 575–604.

Levine, J. & Murrell, D. (2003) The community-level consequences of seed dispersal patterns. *Annual Review of Ecology, Evolution and Systematics*, **34**, 549–574.

Muller-Landau, H.C., Wright, S.J., Calderon, O., Condit, R. & Hubbell, S.P. (2008) Interspecific variation in primary seed dispersal in a tropical forest. *Journal of Ecology*, **96**, 653–667.

Nathan, R. & Muller-Landau, H.C. (2000) Spatial patterns of seed dispersal, their determinants and consequences for recruitment. *Trends in Ecology & Evolution*, **15**, 278–285.

Nathan, R., Safriel, U.N. & Noy-Meir, I. (2001) Field validation and sensitivity analysis of a mechanistic model for tree seed dispersal by wind. *Ecology*, **82**, 374–388.

Nathan, R., Horvitz, N., He, Y., Kuparinen, A., Schurr, F.M. & Katul, G.G. (2011) Spread of North American wind-dispersed trees in future environments. *Ecology Letters*, **14**, 211–219.

Nelder, J.A. & Mead, R. (1965) A simplex method for function minimization. *The Computer Journal*, **7**, 308.

Okubo, A. & Levin, S.A. (1989) A theoretical framework for data analysis of wind dispersal of seeds and pollen. *Ecology*, **70**, 329–338.

Olieman, N.J. & van Putten, B. (2010) Estimation method of multivariate exponential probabilities based on a simplex coordinates transform. *Journal of Statistical Computation and Simulation*, **80**, 355–361.

Prat, D. (1995) Mating system in a clonal Douglas fir (*Pseudotsuga menziesii* (Mirb) Franco) seed orchard. II. Effective pollen dispersal. *Annals of Forest Science*, **52**, 213–222.

R Development Core Team (2011) *R: A Language and Environment for Statistical Computing*. R Foundation for Statistical Computing, Vienna, Austria.

Ribbens, E., Silander, J.A. & Pacala, S.W. (1994) Seedling recruitment in forests: calibrating models to predict patterns of tree seedling dispersion. *Ecology*, **75**, 1794–1806.

Robledo-Arnuncio, J. J. & García, C. (2007) Estimation of the seed dispersal kernel from exact identification of source plants. *Molecular Ecology*, **16**, 5098–5109.

Savage, D., Barbetti, M.J., MacLeod, W.J., Salam, M.U. & Renton, M. (2011) Can mechanistically parameterised, anisotropic dispersal kernels provide a reliable estimate of wind-assisted dispersal? *Ecological Modelling*, **222**, 1673–1682.

Schurr, F.M., Steinitz, O. & Nathan, R. (2008) Plant fecundity and seed dispersal in spatially heterogeneous environments: models, mechanisms and estimation. *Journal of Ecology*, **96**, 628–641.

Skarpaas, O. & Shea, K. (2007) Dispersal patterns, dispersal mechanisms, and invasion wave speeds for invasive thistles. *The American Naturalist*, **170**, 421–430.

Skarpaas, O., Silverman, E.J., Jongejans, E. & Shea, K. (2011) Are the best dispersers the best colonizers? Seed mass, dispersal and establishment in Carduus thistles. *Evolutionary Ecology*, **25**, 155–169.

Soons, M.B. & Bullock, J.M. (2008) Non random seed abscission, long distance wind dispersal and plant migration rates. *Journal of Ecology*, **96**, 581–590.

Soons, M., Messelink, J., Jongejans, E. & Heil, G. (2005) Habitat fragmentation reduces grassland connectivity for both short distance and long distance wind dispersed forbs. *Journal of Ecology*, **93**, 1214–1225.

Soubeyrand, S., Enjalbert, J. & Sache, I. (2008) Accounting for the roughness of circular processes: using Gaussian random processes to model the anisotropic spread of airborne plant disease. *Theoretical Population Biology*, **73**, 92–103.

Soubeyrand, S., Enjalbert, J., Sanchez, A. & Sache, I. (2007) Anisotropy, in direction and in distance, of the dispersal of yellow rust of wheat: experiments in large field plots and estimation. *Phytopathology*, **97**, 1315–1324.

Soubeyrand, S., Enjalbert, J., Kretzschmar, A. & Sache, I. (2009) Building anisotropic sampling schemes for the estimation of anisotropic dispersal. *Annals of Applied Biology*, **154**, 399–411.

Staelens, J., Nachtergale, L., Luyssaert, S. & Lust, N. (2003) A model of wind-influenced leaf litterfall in a mixed hardwood forest. *Canadian Journal of Forest Research*, **33**, 201–209.

Stockmarr, A. (2002) The distribution of particles in the plane dispersed by a simple 3-dimensional diffusion process. *Journal of Mathematical Biology*, **45**, 461–469.

Tackenberg, O. (2003) Modeling long-distance dispersal of plant diaspores by wind. *Ecological Monographs*, **73**, 173–189.

Trakhtenbrot, A., Nathan, R., Perry, G. & Richardson, D.M. (2005) The importance of long distance dispersal in biodiversity conservation. *Diversity and Distributions*, **11**, 173–181.

Tufto, J., Engen, S. & Hindar, K. (1997) Stochastic dispersal processes in plant populations. *Theoretical Population Biology*, **52**, 16–26.

Wagner, S., Walder, K., Ribbens, E. & Zeibig, A. (2004) Directionality in fruit dispersal models for anemochorous forest trees. *Ecological Modelling*, **179**, 487–498.

Wälder, K., Näther, W. & Wagner, S. (2009) Improving inverse model fitting in trees: anisotropy, multiplicative effects, and Bayes estimation. *Ecological Modelling*, **220**, 1044–1053.
Wang, B.C. & Smith, T.B. (2002) Closing the seed dispersal loop. *Trends in Ecology and Evolution*, **17**, 379–385.
Wheeler, J. (1984) A new plot to display the strain of elliptic markers. *Journal of Structural Geology*, **6**, 417–423.
Wright, S.J., Trakhtenbrot, A., Bohrer, G., Detto, M., Katul, G.G., Horvitz, N., Muller-Landau, H.C., Jones, F.A. & Nathan, R. (2008) Understanding strategies for seed dispersal by wind under contrasting atmospheric conditions. *Proceedings of the National Academy of Sciences*, **105**, 19084.

Received 1 November 2011; accepted 20 March 2012
Handling Editor: Jane Molofsky

Supporting Information

Additional Supporting Information may be found in the online version of this article:

Appendix A. Definitions of the Matrushka property, and the 1D and 2D means and quantiles.

Appendix B. Proof that the elliptic distortion model function is well defined, and extensions of the function.

Appendix C. Proof that contour lines in the full elliptic distortion model are non-concentric ellipses and that the elliptic distortion distance fulfils the Matrushka property.

Appendix D. Proof of the form of the two-dimensional dispersal kernel p^{ELL} for the elliptic distortion model.

Appendix E. Principles of the inverse modelling procedure, applied to the elliptic distortion model.

Appendix F. Methods for quantifying directional variability in the elliptic distortion model.

Appendix G. Proofs that the anisotropic models incorporating Von Mises distributions presented in Tufto, Engen & Hindar (1997), Wagner *et al.* (2004) and Staelens *et al.* (2003) are special cases of our framework.

Appendix R. R-code for maximum-likelihood fitting of anisotropic dispersal kernels, specifically elliptic distorted-distance kernels, through inverse modelling.

Appendix S. R-code for simulating datasets similar to the case study dataset, for fitting these datasets and for calculating fit statistics.

As a service to our authors and readers, this journal provides supporting information supplied by the authors. Such materials may be reorganized for online delivery, but are not copy-edited or typeset. Technical support issues arising from supporting information (other than missing files) should be addressed to the authors.